Loss of Basal Cells Precedes Bronchiolitis Obliterans–Like Pathological Changes in a Murine Model of Chlorine Gas Inhalation

Emily G. O'Koren[1], Brigid L. M. Hogan[2], and Michael Dee Gunn[1,3]

[1]Department of Immunology, [2]Department of Cell Biology, and [3]Department of Medicine, Duke University Medical Center, Durham, North Carolina

Bronchiolitis obliterans (BO) is a major cause of chronic airway dysfunction after toxic chemical inhalation. The pathophysiology of BO is not well understood, but epithelial cell injury has been closely associated with the development of fibrotic lesions in human studies and in animal models of both toxin-induced and transplant-induced BO. However, whereas almost all cases and models of BO include epithelial injury, not all instances of epithelial injury result in BO, suggesting that epithelial damage *per se* is not the critical event leading to the development of BO. Here, we describe a model of chlorine-induced BO in which mice develop tracheal and large airway obliterative lesions within 10 days of exposure to high (350 parts per million [ppm]), but not low (200 ppm), concentrations of chlorine gas. Importantly, these lesions arise only under conditions and in areas in which basal cells, the resident progenitor cells for large airway epithelium, are eliminated by chlorine exposure. In areas of basal cell loss, epithelial regeneration does not occur, resulting in persistent regions of epithelial denudation. Obliterative airway lesions arise specifically from regions of epithelial denudation in a process that includes inflammatory cell infiltration by Day 2 after exposure, fibroblast infiltration and collagen deposition by Day 5, and the ingrowth of blood vessels by Day 7, ultimately leading to lethal airway obstruction by Days 9–12. We conclude that the loss of epithelial progenitor cells constitutes a critical factor leading to the development of obliterative airway lesions after chemical inhalation.

Keywords: bronchiolitis obliterans; basal cells; fibrosis; chlorine

CLINICAL RELEVANCE

This report describes a novel murine model of bronchioloitis obliterans (BO), demonstrates the mechanism by which airway fibrotic lesions arise in this model, and proposes that the loss of epithelial progenitor cells is a critical factor in the development of BO. Our conclusions provide significant insights into the pathogenesis of BO, and may suggest therapeutic strategies for this disease.

Bronchiolitis obliterans (BO) is a form of chronic obstructive airway disease in which small airways are compressed and narrowed by fibrosis and inflammation. The resulting fixed airway obstruction leads to dyspnea, typically on exertion, which is often progressive (1–3). BO has numerous causes, including collagen vascular disease, the inhalation of toxic chemicals, viral infections, hematopoietic stem-cell transplantation, and lung transplantation (1). It is the most prominent feature of chronic rejection after lung transplantation, and is the leading cause of death beyond the first year after transplantation (3, 4). In the case of toxin inhalation, BO has been documented after exposures to a wide variety of chemicals, including chlorine, ammonia, methyl isocyanate, mustard gas, and diacetyl, the cause of "popcorn worker's lung" (5, 6). Because diagnosing BO is often difficult, its true incidence may be underestimated. In one recent study, 78% of United States Iraq and Afghanistan veterans who presented with unexplained dyspnea and underwent a lung biopsy showed pathologic evidence of BO, despite, in most cases, normal results of chest x-rays and pulmonary function tests (7).

Pathologically, BO can be divided into two forms: proliferative and constrictive. In proliferative BO, connective tissue breaches the airway lining and then proliferates within the lumen to form tissue masses, akin to granulation tissue (8). This is often seen as an acute inflammation–mediated process, and in some cases responds to corticosteroid treatment (1). In contrast, constrictive BO is an irreversible fibrotic thickening of the submucosa that concentrically constricts the small airways from beneath the airway epithelial lining (1). Constrictive BO responds poorly to treatment, and is associated with high mortality (2, 3). At present, it remains unclear whether constrictive BO is the final outcome of persistent and severe proliferative BO, or whether constrictive and proliferative BO represent distinct responses to differing types of airway injury (9).

The exact pathogenesis of BO remains unclear. In the case of lung transplantation, contributing factors are thought to include innate and adaptive immune responses, tissue ischemia (induced by transplantation and antiendothelial immune responses), and chronic epithelial cell injury (10–13). Several studies suggest that epithelial cell injury is the most critical pathogenic factor. In a mouse model of allogeneic mismatched orthotopic lung transplantation characterized by severe vascular rejection but no epithelial injury, obliterative airway disease did not occur (14). However, in a mouse tracheal transplant model, an alloresponse to epithelium was sufficient to induce obliterative airway disease (10). Similarly, the chronic depletion of mature epithelial cells, either club cells (Clara cells) or Type II alveolar cells, results in abnormal reepithelialization and a fibrotic response (15, 16). Epithelial injury is also a common feature of almost all human instances and animal models of toxic chemical inhalation associated with the development of BO, supporting the view that epithelial damage is a critical factor in the pathogenesis of BO. However, evidence suggests that epithelial injury *per se* is not sufficient for the development of BO. Some

(*Received in original form September 20, 2012 and in final form May 16, 2013*)

This work was supported by the CounterACT Program, the National Institutes of Health Office of the Director, and National Institute of Environmental Health Sciences grant U01ES017219 from the National Institutes of Health.

Correspondence and requests for reprints should be addressed to Michael Dee Gunn, M.D., Department of Immunology, Duke University Medical Center, Box 3547, Durham, NC 27710. E-mail: michael.gunn@duke.edu

This article has an online supplement, which is accessible from this issue's table of contents at www.atsjournals.org

Am J Respir Cell Mol Biol Vol 49, Iss. 5, pp 788–797, Nov 2013

Originally Published in Press as DOI: 10.1165/rcmb.2012-0369OC on June 6, 2013
Internet address: www.atsjournals.org

animal models demonstrate widespread death of epithelial cells, but repair normally, with no evidence of fibrotic lesion development. In animal models that display obliterative airway lesions, both the frequency and the anatomic distribution of these lesions are much less extensive than the epithelial damage. These findings suggest that some factor beyond acute epithelial cell injury is required for the development of BO.

Current animal models of BO include both orthotopic and heterotopic transplantations of tracheas, lungs, and bone marrow (17). In addition, nontransplant models involve the administration of various toxins and the targeted ablation or disabling of epithelial cells (18). Transplant models offer insights into the immune pathogenesis of BO, but in these models, the study of fibrotic responses can be complicated by robust immune response. Mouse models of tracheal transplantation have been criticized for their use of large rather than small airways. However, in terms of size and cellular composition, the mouse trachea is representative of the first six generations of human airways. The mouse trachea, but not its lower airways, contains basal cells that sit beneath the luminal epithelium and function similarly to human airway basal cells in their ability to give rise to epithelial cells during normal homeostasis and after injury (19, 20).

Here, we describe a novel murine model in which obliterative airway lesions with the pathologic appearance of proliferative BO rapidly develop in the tracheas and primary bronchi of mice exposed to high doses of chlorine gas. The sequence of cellular events that occurs during the development of these obliterative airway lesions includes epithelial cell death, the failure of reepithelialization, inflammatory cell infiltration, fibroblast infiltration, collagen deposition, and angiogenesis, ultimately leading to lethal airway obstruction within 10 days. Moreover, in comparing different doses of chlorine exposure, we determined that the BO lesions only develop under conditions and in areas in which basal cells are eliminated by toxic gas exposure. In the absence of basal cells, epithelial regeneration does not occur and regions of epithelial denudation persist, from which an aberrant repair process is initiated that leads to obliterative airway lesions. Our findings suggest that, irrespective of the cause, the loss of epithelial progenitor cells may be a critical factor leading to the development of BO.

MATERIALS AND METHODS

Mice and Survival Studies

We used 8- to 9-week-old C57Bl/6 female mice, purchased from Charles River Laboratories (Wilmington, MA). $CX3CR1^{GFP/GFP}$ mice were provided by D. Littman (New York University, New York, NY), and crossed with C57Bl/6 mice to produce $CX3CR1^{+/GFP}$ mice. All animal experiments were performed in accordance with National Institutes of Health guidelines and protocols approved by the Animal Care and Use Committee at Duke University. *See* the online supplement for further details.

Chlorine Exposure

Briefly, 1% percent Cl_2 in nitrogen was purchased from Airgas National Welders (Research Triangle Park, NC). Mice were restrained and exposed nose-only to Cl_2. Cl_2 concentrations within the chamber were regulated by flow meters from Cole-Palmer (Vernon Hills, IL), regulating 1% Cl_2 gas into filtered air, and set to either 200 parts per million (ppm; low concentration) or 350 ppm (high concentration) for 30 minutes. *See* the online supplement for further details.

Histology and Immunofluorescence

Briefly, tracheas were dissected and fixed in 4% paraformaldehyde. Paraffin and frozen tissues were serially cut (proximal to distal) into transverse sections, and then stained with hematoxylin and eosin or with primary antibodies for immunofluorescence. *See* the online supplement for further details.

Quantification of Epithelium

The length and thickness of tracheal epithelia were measured in photomicrographs of distal tracheal sections, using the ruler function on the LSM image browser (Carl Zeiss, Jena, Germany). All analyzed tracheal sections were cut from the distal trachea. For the quantification of percent epithelialized circumferences on Day 5 after Cl_2, the total distance of tracheal circumference that stained positive for E-cadherin or cytokeratin 5 was divided by the total tracheal circumference as measured along the basal lamina. Epithelial thickness was measured at 200-μm intervals around the total length of E-cadherin$^+$ or cytokeratin 5$^+$ epithelia in each transverse tracheal section. Areas of denuded epithelium were not included in the quantification of thickness.

Sulfosuccinimidobiotin Tracheal Labeling

Mice were restrained and exposed nose-only to either 200 or 350 ppm Cl_2 for 30 minutes. On Day 4 after exposure, mice were anesthetized with intraperitoneal ketamine (100 mg/kg)/xylazine (10 mg/kg), and they then received 0.25 mg of EZ-Link Sulfo-NHS-Biotin, No-Weigh Format (Sulfo-NHS-Biotin; Pierce Biotechnology, Rockford, IL) intranasally at a total of 30 μl. Immediately before administration, Sulfo-NHS-Biotin was reconstituted with molecular-grade water. Tracheas were harvested either 4 hours or 3 days after Sulfo-NHS-Biotin administration (corresponding to Day 4 or Day 7 after Cl_2 exposure, respectively). Tracheas were processed as frozen sections and stained, and then imaged as already described. Quantification methods are further detailed in the online supplement.

Tracheal Cell Isolation and Flow-Cytometric Analysis

Briefly, excised tracheas were digested into a single-cell suspension, counted, stained, and analyzed using a LSRII flow cytometer (BD Pharmingen, San Jose, CA) (*see* the online supplement for details)

Statistical Analysis

Numerical data are presented as means, means ± SDs, or means ± SEMs, as indicated in figure legends. The comparison between survival curves was performed with the log-rank test, using GraphPad Prism software (GraphPad, San Diego, CA). All data were analyzed by Student *t* tests using GraphPad Prism software, as indicated in figure legends. Pearson correlation coefficients were generated using GraphPad Prism software.

RESULTS

Obliterative Airway Lesions Develop in Mice Exposed to High-Dose Cl_2

We developed a model of Cl_2-induced lung injury in which up to six mice can be simultaneously exposed to a given concentration of Cl_2 gas by nose-only inhalation (Figure E1 in the online supplement). In preliminary dose-ranging experiments, we determined that exposure to 175–250 ppm Cl_2 for 30 minutes resulted in minimal acute mortality. However, during our experiments, we observed that a small number of mice exposed to Cl_2 appeared to recover symptomatically from the acute effects of Cl_2, but then developed severe respiratory distress requiring euthanasia on Days 6–12. A similar unexplained late mortality in Cl_2-exposed mice has been described previously (21). To explore this phenomenon further, mice were exposed to a higher dose of Cl_2 (350 ppm for 30 minutes). Rather than recover, 75% of mice exposed to 350 ppm Cl_2 developed a distinct pattern of labored breathing between Days 6 and 12, which progressed to severe respiratory distress requiring euthanasia within 24 hours (Figure 1A). In comparison, only 16% of mice exposed to 200 ppm Cl_2 required euthanasia (Figure 1A). On pathological examination, all of the mice that developed labored breathing displayed grossly visible obliterative airway lesions. These lesions occurred most commonly in the lower third of the trachea and in the mainstem

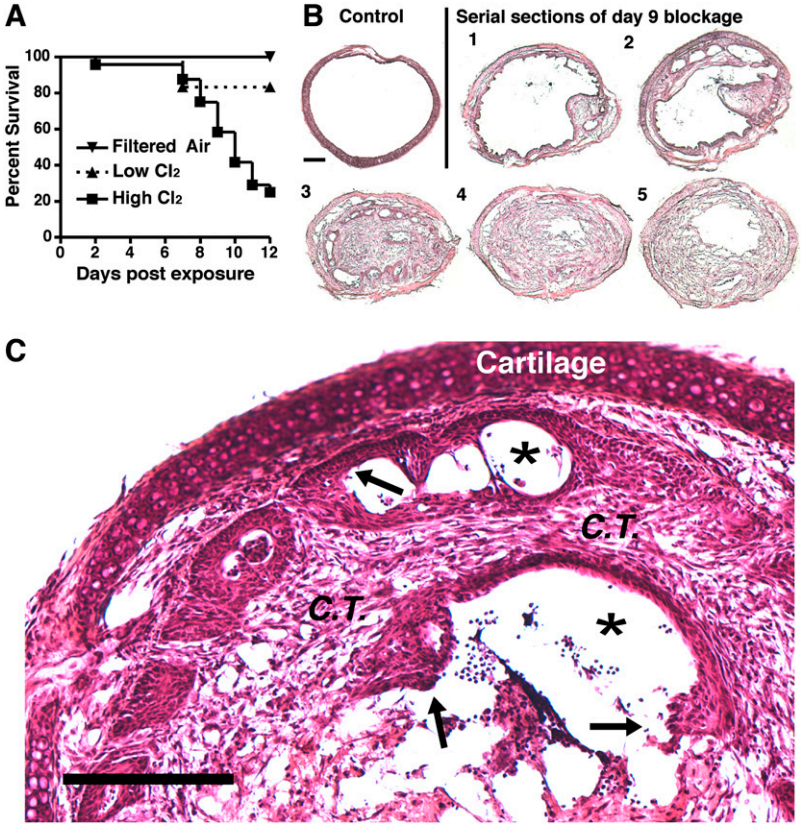

Figure 1. High concentrations of Cl_2 induce lethal obliterative airway lesions. (*A*) Survival after exposure to filtered air ($n = 3$ mice), low-dose Cl_2 (200 parts per million [ppm], $n = 6$), or high-dose Cl_2 (350 ppm, $n = 24$). $P = 0.0337$ between high-dose and low-dose survival curves, according to log-rank test. (*B*) Transverse sections from an unexposed trachea and a mouse killed 9 days after high-dose Cl_2. *Serial sections 1–5* indicate anterior to posterior order. Sections are representative of 16 tracheas similarly examined. *Scale bar*, 200 μm. (*C*) Day 9 blockage exhibits abnormal reepithelialization (*arrows*), connective tissue (*C.T.*) invasion, and the nearly complete occlusion of the lumen (*asterisks*). *Scale bar*, 200 μm.

bronchi, and had the appearance of granulation tissue. In transverse histological sections of the tracheas, obliterative airway lesions occluded more than 80% of the airway lumen (Figure 1B). These obliterative lesions contained both connective tissue and inflammatory cells, and displayed incomplete epithelial coverage at the lesion/airway interface (Figure 1C). Overall, the cellular composition and appearance of these lesions closely resembled the histopathology of human proliferative BO lesions (22).

Lesion Formation Coincides with Basal Cell but Not Luminal Epithelial Cell Death

To determine whether the increased frequency of obliterative airway lesions in mice exposed to 350 ppm Cl_2 was attributable to more severe epithelial injury in these animals, we compared the fate of airway epithelia in mice exposed to low-dose (200 ppm) and high-dose (350 ppm) Cl_2. Three hours after low-dose Cl_2 exposure, tracheas displayed large regions in which luminal epithelial cells (ciliated and club cells) were necrotic and beginning to slough off (Figures 2B and 2H). By 24 hours, the necrotic epithelia sloughed off, revealing a thin layer of simple squamous cells (Figures 2C and 2I). In contrast, 3 hours after high-dose Cl_2 exposure, many regions contained luminal epithelial cells that were swollen and lacked cilia, but remained attached to the tracheal wall (Figures 2D and 2K). By 24 hours, the epithelia were still attached but clearly necrotic. They displayed widespread cellular swelling and loss of nuclei (Figures 2E and 2L). During the next 10 days, the great majority of mice exposed to low-dose Cl_2 displayed complete epithelial repair with no evidence of fibrotic lesions (data not shown), whereas mice exposed to high-dose Cl_2 developed obliterative airway lesions.

These findings suggest that acute epithelial damage alone is not sufficient to induce obliterative airway lesions. This view is consistent with our findings in a different model of toxic chemical exposure, namely, SO_2 inhalation, which we previously described in detail (19, 23). As with 200 ppm Cl_2, mice exposed to SO_2 displayed widespread luminal epithelial necrosis, the sloughing of epithelium revealing a layer of simple squamous cells, and complete epithelial repair after 14 days, with no evidence of obliterative lesion formation (19). In this model, we observed that tracheal basal cells survived SO_2 exposure, proliferated, and gave rise to relatively large patches of descendants that included both club and ciliated cells, thus acting as the progenitor cells for tracheal epithelia after chemical injury. Recent evidence suggests that basal cells also act as the progenitor cells for epithelial repair after Cl_2 inhalation (24).

To determine whether the differences in epithelial repair we observed in mice exposed to low versus high doses of Cl_2 were attributable to differences in basal cell survival, we examined tracheas for the presence of basal cells after low-dose and high-dose Cl_2 exposure. Immunohistochemical staining with anti–E-cadherin marked both luminal epithelial and basal cells. To identify basal cells specifically, we costained with anti–cytokeratin 5, a basal cell–specific marker. Our analysis demonstrated that basal cells remained viable and were present in normal numbers, relative to unexposed mice, after low-dose Cl_2 exposure (Figures 2G and 2J). In these sections, most of the mature columnar, luminal epithelium (E-cadherin$^+$ and cytokeratin 5$^-$) was absent, and the epithelium replacing it consisted primarily of basal cells (E-cadherin$^+$ and cytokeratin 5$^+$). In contrast, mice exposed to high-dose Cl_2 displayed numerous large areas of trachea that were completely devoid of cytokeratin 5$^+$ basal cells (Figure 2M). The epithelial cells in these regions remained attached, were swollen, and displayed faint E-cadherin$^+$ staining, but no longer exhibited nuclei at 24 hours after injury (Figure 2L). These findings strongly suggest that the chemical-induced loss of basal cells is a critical event in the course of toxin exposure. If basal cells remain viable, they are known to serve

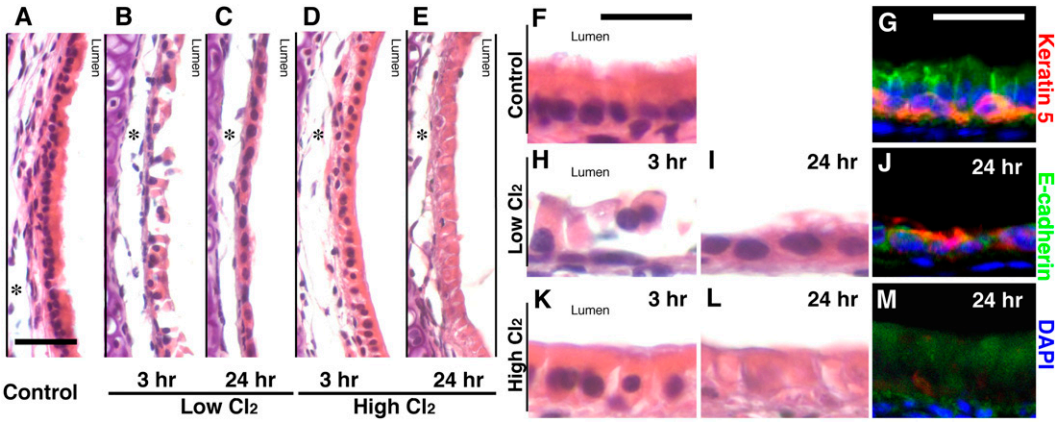

Figure 2. Exposure to high-dose Cl_2 results in basal cell death. Photomicrographs depict hematoxylin-and-eosin–stained tracheas from an unexposed mouse (*A* and *F*), or after low-dose Cl_2 at 3 hours (*B* and *H*) and 24 hours (*C* and *I*), or after high-dose Cl_2 at 3 hours (*D* and *K*) and 24 hours (*E* and *L*). Immunofluorescent staining is also shown of uninjured trachea (*G*), 24 hours after low-dose (*J*) and high-dose (*M*) Cl_2. E-cadherin, *green*; cytokeratin 5, *red*; 4′,6-diamidino-2-phenylindole (DAPI), *blue*. All images are representative of 5–6 tracheas at each time. *Scale bars*, 20 μm for *A–E* and 25 μm for *F–M*. *Asterisks* denote fixation artifacts.

as a source of progenitor cells for rapid epithelial repair. Here, we propose that in the absence of basal cells, reepithelialization does not occur, and a fibrotic response is initiated.

Basal Cell Loss Correlates with Reduced Tracheal Reepithelialization

To determine the consequences of basal cell loss on epithelial repair, inflammation, and fibrosis, we examined the time course of these events in mice exposed to low-dose and high-dose Cl_2. In general, normal epithelial repair is thought to occur in three stages (25–27). First, basal cells spread and migrate to cover denuded epithelium. Second, these cells proliferate, with self-renewing basal cells remaining near the basal lamina and daughter cells forming upper layers of transitory squamous metaplasia. Lastly, the upper layers remodel to form a pseudostratified layer of mature, differentiated mucociliary epithelium.

By Day 5 after Cl_2 exposure, low-dose and high-dose Cl_2-exposed tracheas clearly undergo markedly different rates of epithelial repair. After low-dose Cl_2 exposure, the entire trachea is reepithelialized. The thickened E-cadherin$^+$ luminal epithelium with basal cells (E-cadherin$^+$ cytokeratin 5$^+$) residing near the basal lamina is characteristic of the second phase of epithelial repair (Figure 3A). No evidence of cellular migration into the lumen was observed. In contrast, by Day 5 after high-dose Cl_2 exposure, necrotic epithelium is no longer attached to the airway wall, but on average, 49% of the tracheal circumference lacks both mature epithelium and basal cells, as indicated by the absence of E-cadherin and cytokeratin 5 staining (Figures 3B, *insets 4* and *6*, and 3F). In those areas that do contain epithelium, it consists of a single layer of cells, some of which are cytokeratin 5$^+$, indicating the presence of basal cells (Figure 3B, *insets 3* and *5*). On average, this epithelium is 50% less thick than after low-dose Cl_2 exposure (Figure 3E). These observations suggest that even in areas where basal cells survive, their decreased numbers or reduced function significantly retard epithelial repair. In large areas of epithelial necrosis caused by high-dose Cl_2, the basal lamina is exposed to the lumen, whereas after low-dose Cl_2 exposure, it is covered by regenerating epithelium (Figures 3C and 3D). In addition, by Day 3 after high-dose Cl_2 exposure, the necrotic epithelium that initially remained adherent to the tracheal wall becomes displaced into the lumen, where it is retained as a mass of necrotic cells (Figure 3D).

By Day 7 after low-dose Cl_2 exposure, the trachea remains fully epithelialized. Most of the transitory squamous metaplasia has remodeled into normal pseudostratified epithelium (Figures 3G and 3I). In contrast, after high-dose Cl_2, the epithelium forms disorganized patches, varying in stages of repair (Figures 3H and 3J). In some areas, connective tissue has fused with the trachea wall, preventing the reepithelialization of the original basal lamina. In addition, the epithelium has begun surrounding the invading connective tissue in places, but denuded areas remain where obliterative lesions interface directly with the airspace.

Obliterative Lesions Originate from Areas of Denuded Epithelium

Although these findings demonstrate an overall association between the occurrence of epithelial denudation and the formation of obliterative airway lesions, they do not directly demonstrate that obliterative lesions arise from areas of epithelial denudation. To address this issue, we developed a technique that would allow us to track the fate of individual lesions in individual animals. To label areas of epithelial denudation, we administered sulfosuccinimidobiotin (Sulfo-NHS-Biotin) to mice intranasally, 4 days after low-dose or high-dose Cl_2 exposure. Sulfo-NHS-Biotin is comprised of esters of biotin that are highly reactive and cell-impermeable, and that form stable amide bonds with primary amines found on the surfaces of living and nonliving organic material (28). To confirm that this technique specifically labels areas of epithelial denudation, tracheas were harvested 4 hours after Sulfo-NHS-Biotin administration (on Day 4 after exposure) and stained with anti–E-cadherin and streptavidin, to localize intact epithelium and covalent biotin attachment, respectively.

All tracheas harvested 4 hours after Sulfo-NHS-Biotin administration demonstrated uniform staining for biotin on their epithelial surfaces. In addition, we observed the biotin staining of exposed basement membrane areas and/or subepithelial connective tissue that was highly dependent on the presence and extent of epithelial denudation. Tracheas with no visible epithelial denudation typically displayed one or more small areas of subepithelial biotin staining (Figure 4A), the total length of which averaged 390 ± 281 μm (Figure 4E). In contrast, tracheas with visible regions of epithelial denudation typically displayed one large area of subepithelial biotin staining (Figure 4B), the total length of which averaged 2,411 ± 1,070 μm (Figure 4E). The length of subepithelial staining in

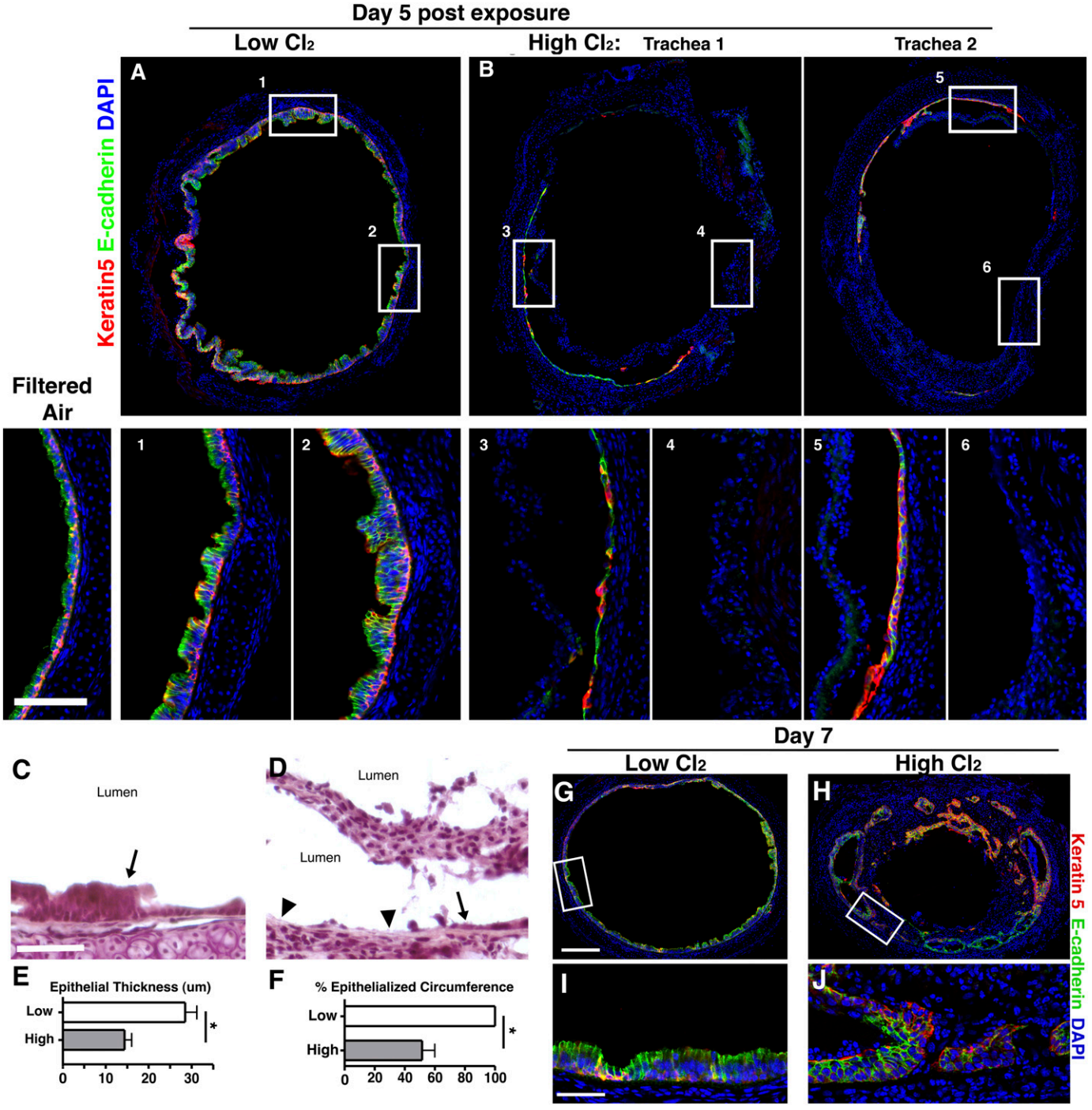

Figure 3. Basal cell loss results in aberrant reepithelialization. Immunofluorescent staining of epithelium is depicted 5 days after low-dose (*A*) or high-dose (*B*) Cl_2. Two individual tracheas are shown in *B*. *Boxed areas* in the *top row* are magnified in the *bottom row*, and correspond by number. E-cadherin, *green*; cytokeratin 5, *red*; DAPI, *blue*. *Scale bar*, 200 μm. Hematoxylin-and-eosin staining of epithelium is shown 5 days after low-dose (*C*) or high-dose (*D*) Cl_2. Epithelium is denoted by *arrows*, and denuded epithelium by *arrowheads*. *Scale bar*, 50 μm. Quantification of percent epithelialized tracheal circumference (*E*) and epithelial thickness (*F*) is shown 5 days after exposure to low-dose or high-dose Cl_2 ($n = 3$; $^*P < 0.05$ according to Student *t* test; data are presented as means ± SEMs). Immunofluorescent staining of epithelium is shown 7 days after low-dose (*G* and *I*) or high-dose (*H* and *J*) Cl_2. *Scale bar*, 200 μm for *G* and *H*. *Scale bar*, 25 μm for *I* and *J*. All images are representative of 5–6 tracheas at each time.

individual mice was closely correlated with the length of associated epithelial denudation (Figure 4F; $r = 0.920$, $P < 0.0001$). Moreover, the length of this subepithelial staining, when measured from the center of epithelial denudation, either equaled or slightly exceeded the length of epithelial denudation (Figure 4G). These results demonstrate that Sulfo-NHS-Biotin staining accurately labels the extent and position of epithelial denudation.

To determine whether obliterative airway lesions arise from areas of epithelial denudation in individual mice, a separate experiment was performed in which mice were exposed, as before, to low-dose or high-dose Cl_2, and they then received Sulfo-NHS-Biotin after 4 days. In this experiment, however, the tracheas were harvested 3 days later rather than at 4 hours, to allow time for repair or lesion formation. In these samples, the surface

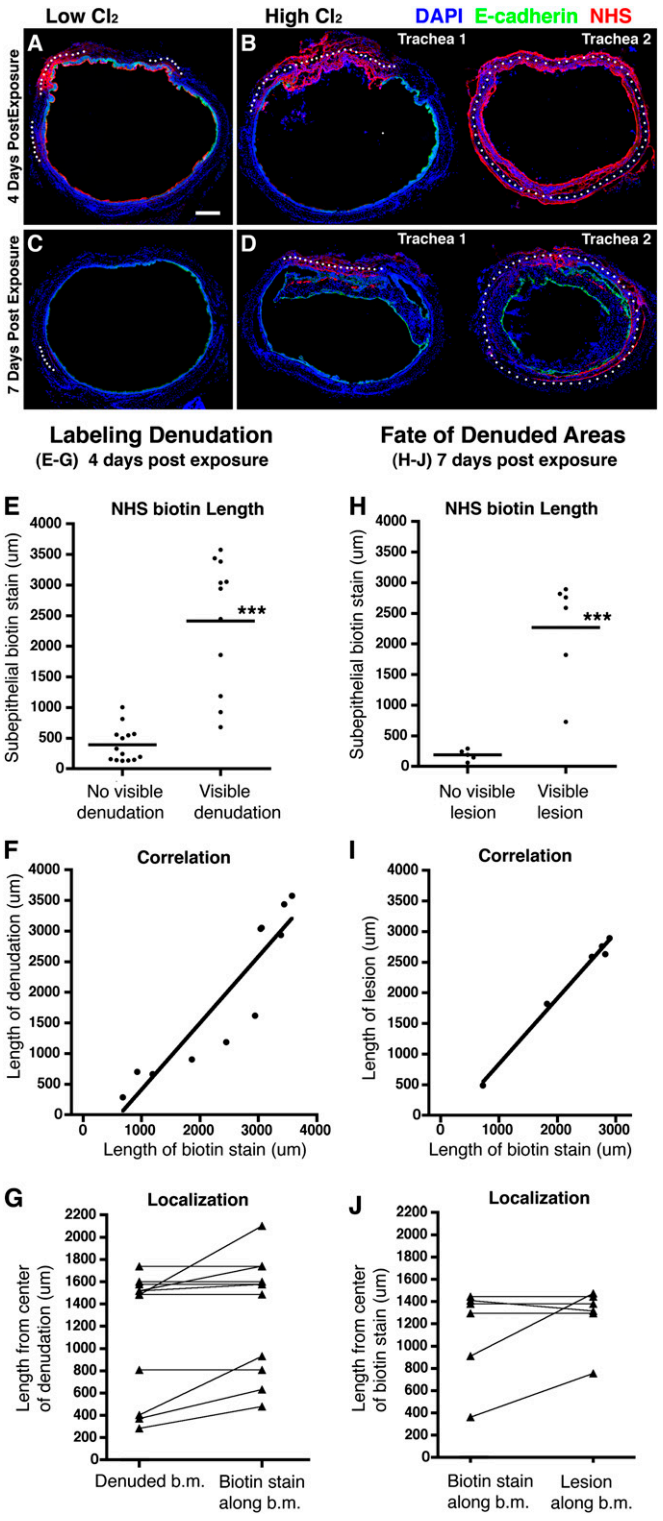

Figure 4. Tracheal blockages originate from areas of denuded epithelium. Mice were exposed to low-dose or high-dose Cl_2, and then intranasally received the labeling agent Sulfo-NHS-Biotin (NHS) 4 days after exposure. (*A* and *B*) Immunofluorescent staining of E-cadherin and biotin 4 hours after the administration of NHS-Biotin in mice that were exposed to low-dose or high-dose Cl_2. Images are representative of multiple tracheas. Low-dose Cl_2, $n = 5$. High-dose Cl_2, $n = 10$ (two examples are shown in *B*). (*C* and *D*) Immunofluorescent staining of E-cadherin and biotin was performed 3 days after biotin labeling (*7* days after exposure to low-dose or high-dose Cl_2). Images are representative of multiple tracheas. Low-dose Cl_2, $n = 3$. High-dose Cl_2, $n = 7$ (two examples are shown in *D*). *Scale bar*, 200 μm. *White dots* mark regions of subepithelial biotin staining. The lengths of these regions were measured along the basement membrane for quantitation. (*E*) The length of subepithelial biotin staining in areas with or without visible denudation ($n = 15$ tracheas). ***$P < 0.0001$, according to Student *t* test. (*F*) Correlation between length of biotin staining and the length of epithelial denudation ($r = 0.920$, $P < 0.0001$; $n = 10$ tracheas). (*G*) The length of biotin staining in areas of denuded epithelium was measured from the center of the denuded area outward in each direction. For each data point, the length is an average of the left and right extensions ($n = 10$ tracheas). b.m., basement membrane. (*H*) The length of subepithelial biotin staining in areas with or without visible lesions ($n = 10$ tracheas; ***$P < 0.0001$, according to Student *t* test). (*I*) Correlation between length of biotin staining and the length of luminal lesions ($r = 0.995$, $P < 0.0001$; $n = 6$ tracheas). (*J*) The length of lesions measured from the center of the associated biotin staining outward in each direction. For each data point, the length is an average of the left and right extensions ($n = 6$ tracheas).

staining of airway epithelial cells was not detected, probably because of the membrane turnover of labeled live cells, but areas of subepithelial staining remained visible. No intraluminal lesions were found in sections that contained less than 300 μm of subepithelial staining, suggesting that the development of such lesions requires a certain amount of epithelial denudation (Figure 4H). In contrast, all sections with more than 300 μm of subepithelial staining contained intraluminal lesions. In individual mice, the length of tracheal wall covered by intraluminal lesions was closely correlated with the length of subepithelial staining (Figure 4I; $r = 0.995$, $P < 0.0001$). Lesions, when measured from the center of biotin staining, typically equaled or slightly exceeded the length of the associated biotin stain (Figure 4J). These findings demonstrate that intraluminal lesions arise from areas of epithelial denudation, and suggest that the size of intraluminal lesions is determined by the extent of epithelial denudation.

We also graphed the data points in Figures 4E and 4H in a manner that reflects the exposure group from which each data point was generated (Figure E2). Data points representing short lengths of biotin staining and associated with no visible denudation or lesions were primarily generated after exposure to low-dose Cl_2. In contrast, data points representing long lengths of biotin staining and associated with visible denudation or lesions were primarily generated after exposure to high-dose Cl_2.

Inflammatory Cell Infiltration Precedes Airway Intraluminal Fibrosis

To better define the specific cellular events associated with the development of intraluminal lesions, we examined the time-course of inflammation, collagen production, and vascularization in mice exposed to 350 ppm Cl_2. By Day 2 after exposure, $CD11b^+$ cells, consisting of both neutrophils and macrophages, began to infiltrate the dead epithelium (Figures 5A and 5B). By Day 5, infiltration by $CD11b^+$ cells was substantial (Figure 5G), with macrophages (Figure 5F, *arrowheads*) and neutrophils (Figure 5F, *arrows*) comprising the predominant cell types (Figures 5E and 5F). By Day 7, $CD11b^+$ cell infiltrates decreased (Figures 5I–5K), but in many cases reappeared when mice developed terminal respiratory distress on or around Day 9 (Figures 5M–5O). Higher-magnification images of CD11b and collagen I staining are provided in Figure E3.

To quantify these inflammatory cell infiltrates, whole tracheas from mice exposed to low-dose or high-dose Cl_2 were digested

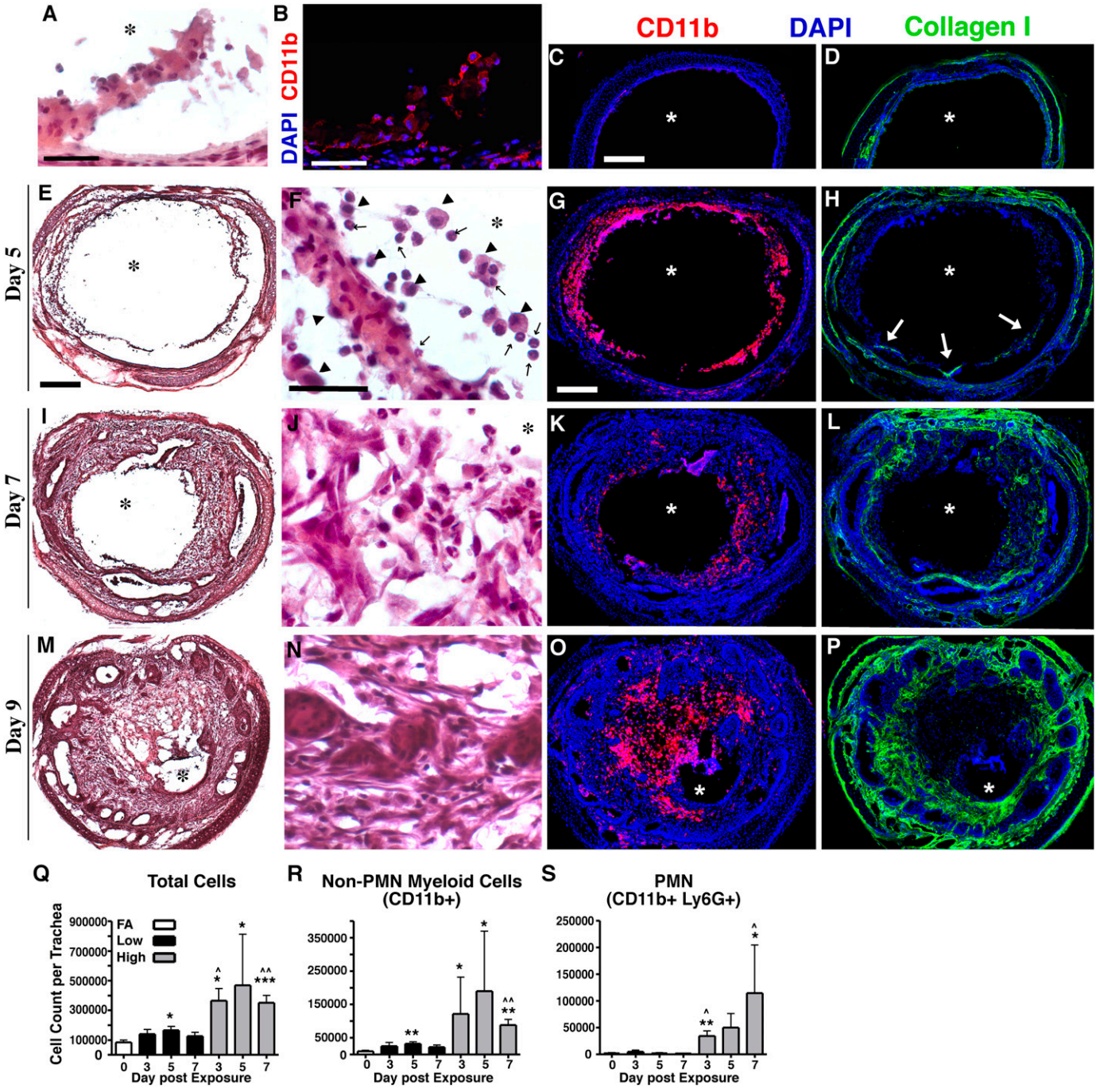

Figure 5. Loss of epithelial integrity results in inflammatory cell infiltration, mesenchyme infiltration, and collagen deposition. (*A*) Hematoxylin-and-eosin staining of tracheal epithelium, 2 days after exposure to high-dose Cl_2. (*B*) Immunofluorescent staining for CD11b (*red*) in a similar Day 2 tissue section. In *A* and *B*, *scale bars*, 25 μm. Immunofluorescent staining of either CD11b (*red*) or collagen I (*green*) in a control tracheal section and sections harvested on Days 5, 7, and 9 after high-dose Cl_2 and CD11b (*C*, *G*, *K*, and *O*, respectively) and collagen I (*D*, *H*, *L*, and *P*, respectively; *scale bar*, 200 μm). In *H*, *arrows* denote collagen 1^+ cells infiltrating the lumen. Hematoxylin-and-eosin staining of tracheal sections harvested on Days 5, 7, and 9 after high-dose Cl_2 (*E*, *I*, and *M*, respectively; *scale bar*, 200 μm); magnified images are presented *F*, *J*, and *N*, respectively (*scale bar*, 25 μm) In *F*, *arrowheads* denote macrophages, whereas *arrows* denote neutrophils. All tissue sections are representative of 5–6 tracheas at each time. *Asterisks* denote the lumen. Using flow cytometry, total cells (*Q*), non-neutrophil $CD11b^+$ cells (*R*), and neutrophils (*S*) were quantified from tracheal digests of mice exposed to filtered air (FA), low-dose, or high-dose Cl_2. *Bars* represent means ± SDs for 5–8 mice per group. $^*P < 0.05$, $^{**}P < 0.005$, and $^{***}P < 0.0001$, in comparison with FA according to Student *t* test. $^{\wedge}P < 0.05$ and $^{\wedge\wedge}P < 0.005$, in comparison with day-matched low-dose Cl_2, according to Student *t* test. PMN, polymorphonuclear leukocyte.

into single-cell suspensions, and then subjected to flow cytometric analysis. In mice exposed to low-dose Cl_2, the numbers of total tracheal cells and monocytes/macrophages ($CD11b^+$ $Ly6G^-$) were significantly increased on Day 5 only, with no increase in neutrophils (Figures 5Q–5S). In mice exposed to high-dose Cl_2, the numbers of total tracheal cells and monocytes/macrophages were significantly increased at all time points, and the number of neutrophils significantly increased on

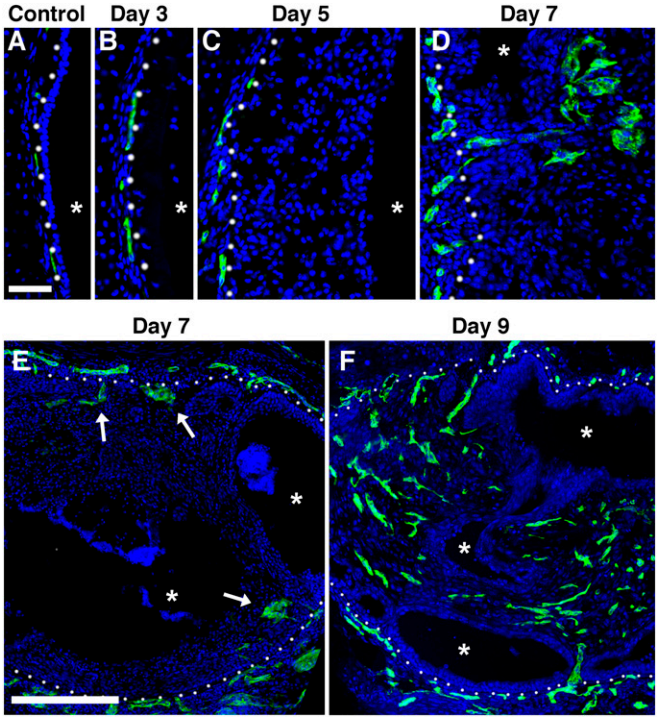

Figure 6. Vascularization of tracheal blockages. Immunofluorescent staining of endothelial cells (platelet endothelial cell adhesion molecule, *green*) in an uninjured trachea (*A*) and in tracheas harvested 3 (*B*), 5 (*C*), 7 (*D* and *E*), and 9 (*F*) days after exposure to high-dose Cl_2. *Whites dots* denote the basal lamina. *Arrows* denote endothelial sprouts into the lumen. *Asterisks* denote the lumen. Tissue sections are representative of 5–6 tracheas at each time. *Top, scale bar*: 50 μm. *Bottom, scale bar*: 200 μm.

Days 3 and 7 (Figures 5Q–5S). These findings demonstrate that inflammatory cell infiltration, especially of monocytes/macrophages, precedes the development of intraluminal lesions, which are typically observed on Day 7 after Cl_2 exposure.

At the time when the infiltration of monocytes/macrophages is peaking, around Day 5 after exposure, collagen-producing cells begin to infiltrate the cellular mass (Figure 5H, *arrows*). After this begins, the deposition of collagen-producing fibroblasts and connective tissue within the airway lesion increases rapidly (Figures 5F, 5H, 5J, 5L, 5N, and 5P). Consequently, tracheas can progress from being totally patent to almost totally occluded during a period of 4 days (Figures 5E, 5I, and 5M).

Vascularization of Obliterative Airway Lesions Is a Late Event

To determine whether vascularization plays a significant role in the development of obliterative airway lesions, we performed immunohistochemistry for the endothelial cell (EC) marker platelet endothelial cell adhesion molecule on tissue sections during the course of lesion development. Before exposure, tracheal blood vessels lay just below the basal lamina (Figure 6A). ECs remained in this position through Day 5 after Cl_2 exposure (Figures 6B and 6C). By Day 7, ECs began to penetrate the basal lamina into the developing obliterative lesions (Figures 6D and 6E, *arrows*). This corresponded to the time of rapidly increasing cellularity within obliterative lesions. By Day 9, obliterative airway lesions were highly vascularized (Figure 6F). These findings suggest that vascularization does not play a role in the initiation of obliterative airway lesions.

DISCUSSION

BO is a debilitating and potentially lethal disease resulting from the narrowing of the airways by fibrosis and inflammation. The pathogenesis of BO is not clearly understood, but may involve immune components, tissue ischemia, and epithelial damage (15, 22). The majority of BO cases, animal and human, include epithelial damage, but not all cases of epithelial damage result in BO. Here, we find that a loss of basal cells is closely associated with the development of obliterative airway lesions in a model of acute toxin-induced airway injury. This conclusion is based on several findings. First, we demonstrate that the extent of acute injury to luminal epithelial cells does not correlate with the development of obliterative airway lesions. Second, we find that the development of such lesions occurs only under conditions and in areas in which basal cells are eliminated. Third, we find that the loss of basal cells is closely associated with a failure to reepithelialize regions of epithelial denudation. Fourth, we find that obliterative airway lesions arise only at sites of epithelial denudation, and that the size of such developing lesions is closely correlated with the extent of epithelial denudation. To our knowledge, this is the first demonstration that intraluminal fibrotic lesions arise specifically at sites of epithelial denudation. Taken together, our findings suggest a clear mechanism by which a loss of basal cells leads to airway intraluminal fibrosis. This mechanism is consistent with human pathological studies in which obliterative airway lesions appeared to arise from areas of epithelial denudation (22).

Although our findings demonstrate strong correlations among basal cell loss, persistent regions of epithelial denudation, and the development of airway intraluminal fibrosis, they do not directly prove that basal cell loss is the cause of airway intraluminal fibrosis. Such proof will likely require the targeted preservation or elimination of basal cells in an animal model. However, several other associative studies have been performed that support our overall conclusion. Only some toxic chemical exposures are known to lead to the development of BO. Our findings suggest that the ability of individual chemicals to cause BO is directly related to their effects on basal cells. Although data on the toxicity of specific chemicals toward basal cells are limited, the available studies support this conclusion. In animal models, chemicals such as naphthalene, nolidocanol, and SO_2 do not cause basal cell loss, and do not cause airway intraluminal fibrosis (29). In contrast, exposures to diacetyl and sulfur mustard, which are known to cause BO, have been shown to cause basal cell depletion (30, 31). For any given chemical, a dosage effect will also occur, as demonstrated by our comparison of Cl_2 dosages. In addition, a recent study comparing Cl_2-induced lung injury in FVB/NJ and A/J mice found that reduced epithelial repair and increased airway fibrosis were associated with a reduced number of resident basal cells at baseline (24, 32). Taken together, our findings and previous reports demonstrate a clear association between basal cell loss and the development of obliterative airway lesions.

According to our model, the loss of basal cells does not directly stimulate obliterative airway lesion formation. Rather, the failure of reepithelialization and the consequent prolonged presence of regions of complete epithelial denudation stimulate an intraluminal fibrotic response. This view is consistent with previous studies in which epithelial denudation induced by a chronic depletion of mature epithelial cells resulted in the development of BO-like fibrotic lesions (15, 16). After chronic Clara cell (club cell) depletion, intrabronchiolar fibrotic lesions only arose in areas of complete epithelial denudation, whereas peribronchiolar fibrosis arose in areas that maintained epithelial integrity, despite persistent epithelial injury. Pathologically, intrabronchiolar and peribronchiolar fibrosis are similar to

human proliferative and constrictive BO, respectively. These observations suggest that the development of proliferative versus constrictive BO may depend on the extent and timing of epithelial injury. Proliferative BO may also advance to constrictive BO. In a nitric acid–induced rat model of BO, proliferative lesions were observed after the first week of injury, followed by the occurrence of constrictive BO (33). We were unable to address the possibility of a transition from one pathology to another in our model, because all mice that survived high-dose Cl_2 exposure displayed fully reepithelialized their tracheas 2–3 weeks after injury, with no evidence of fibrosis (data not shown). We assume these mice retained enough surviving basal cells to repair normally, and avoid the initiation of proliferative BO.

Although our findings directly apply only to proximal airway regions that contain basal cells, the depletion of other types of epithelial progenitor cells in distal airways likely also leads to intraluminal fibrotic lesions. Human pathological studies demonstrate that such lesions arise by connective tissue penetrating areas of epithelial denudation (22). Several types of distal airway and alveolar epithelial progenitor cells have been described that are distinct from basal cells (34). To determine whether such cells are depleted by stimuli that lead to distal airway or alveolar intraluminal fibrosis would be of interest. This would include exposure to chemicals such as phosgene and chloropicrin that preferentially target the distal lung. It would also include non–toxin-related causes of BO. For example, in lung transplantation–induced BO, immune-mediated epithelial progenitor cell death may contribute to aberrant repair processes and fibrosis. Similarly, the tissue ischemia associated with lung transplantation may be extensive enough to eliminate epithelial progenitor cells.

The model of Cl_2-induced airway injury we describe causes the reproducible ablation of basal cells, followed by the rapid development of obliterative airway lesions. Relative to other models of BO, this model offers several advantages. It is relatively simple, requires no surgery, is highly reproducible, and results in the near-total occlusion of airways within 10–12 days. The exposure of mice to high-dose Cl_2 induces a well-demarcated series of pathological changes that will allow for a more detailed analysis of the individual cellular and molecular events that lead from basal cell loss to airway occlusion. Because this model uses C57BL/6 mice, it is readily amenable to analysis using the large number of genetically altered mouse strains available in this background. We anticipate that this model will prove useful in elucidating the pathophysiology of proliferative BO and in the identification of potential therapies for this disease.

Author disclosures are available with the text of this article at www.atsjournals.org.

References

1. Epler GR. Constrictive bronchiolitis obliterans: the fibrotic airway disorder. *Expert Rev Respir Med* 2007;1:139–147.
2. Egan JJ. Obliterative bronchiolitis after lung transplantation: a repetitive multiple injury airway disease. *Am J Respir Crit Care* 2004;170:931–932.
3. Scott AI, Sharples LD, Stewart S. Bronchiolitis obliterans syndrome: risk factors and therapeutic strategies. *Drugs* 2005;65:761–771.
4. Kuo E, Bharat A, Dharmarajan S, Fernandez F, Patterson GA, Mohanakumar T. Animal models for bronchiolitis obliterans syndrome following human lung transplantation. *Immunol Res* 2005;33:69–81.
5. Boswell RT, McCunney RJ. Bronchiolitis obliterans from exposure to incinerator fly ash. *J Occup Environ Med* 1995;37:850–855.
6. Palmer SM, Flake GP, Kelly FL, Zhang HL, Nugent JL, Kirby PJ, Foley JF, Gwinn WM, Morgan DL. Severe airway epithelial injury, aberrant repair and bronchiolitis obliterans develops after diacetyl instillation in rats. *PLoS ONE* 2011;6:e17644.
7. King MS, Eisenberg R, Newman JH, Tolle JJ, Harrell FE Jr, Nian H, Ninan M, Lambright ES, Sheller JR, Johnson JE, *et al*. Constrictive bronchiolitis in soldiers returning from Iraq and Afghanistan. *N Engl J Med* 2011;365:222–230.
8. Epler GR. Bronchiolitis obliterans organizing pneumonia, 25 years: a variety of causes, but what are the treatment options? *Expert Rev Respir Med* 2011;5:353–361.
9. King TE Jr. Overview of bronchiolitis. *Clin Chest Med* 1993;14:607–610.
10. Fernandez FG, Jaramillo A, Chen C, Liu DZ, Tung T, Patterson GA, Mohanakumar T. Airway epithelium is the primary target of allograft rejection in murine obliterative airway disease. *Am J Transplant* 2004;4:319–325.
11. Babu AN, Murakawa T, Thurman JM, Miller EJ, Henson PM, Zamora MR, Voelkel NF, Nicolls MR. Microvascular destruction identifies murine allografts that cannot be rescued from airway fibrosis. *J Clin Invest* 2007;117:3774–3785.
12. Snell GI, Westall GP. The contribution of airway ischemia and vascular remodelling to the pathophysiology of bronchiolitis obliterans syndrome and chronic lung allograft dysfunction. *Curr Opin Organ Transplant* 2010;15:558–562.
13. Ropponen JO, Syrjala SO, Krebs R, Nykanen A, Tikkanen JM, Lemstrom KB. Innate and adaptive immune responses in obliterative airway disease in rat tracheal allografts. *J Heart Lung Transplant* 2011;30:707–716.
14. Okazaki M, Gelman AE, Tietjens JR, Ibricevic A, Kornfeld CG, Huang HJ, Richardson SB, Lai J, Garbow JR, Patterson GA, *et al*. Maintenance of airway epithelium in acutely rejected orthotopic vascularized mouse lung transplants. *Am J Respir Cell Mol Biol* 2007;37:625–630.
15. Perl AK, Riethmacher D, Whitsett JA. Conditional depletion of airway progenitor cells induces peribronchiolar fibrosis. *Am J Respir Crit Care Med* 2011;183:511–521.
16. Sisson TH, Mendez M, Choi K, Subbotina N, Courey A, Cunningham A, Dave A, Engelhardt JF, Liu X, White ES, *et al*. Targeted injury of Type II alveolar epithelial cells induces pulmonary fibrosis. *Am J Respir Crit Care Med* 2010;181:254–263.
17. Sato M, Keshavjee S, Liu M. Translational research: animal models of obliterative bronchiolitis after lung transplantation. *Am J Transplant* 2009;9:1981–1987.
18. De Vleeschauwer S, Vanaudenaerde B, Vos R, Meers C, Wauters S, Dupont L, Van Raemdonck D, Verleden G. The need for a new animal model for chronic rejection after lung transplantation. *Transplant Proc* 2011;43:3476–3485.
19. Rock JR, Onaitis MW, Rawlins EL, Lu Y, Clark CP, Xue Y, Randell SH, Hogan BL. Basal cells as stem cells of the mouse trachea and human airway epithelium. *Proc Natl Acad Sci USA* 2009;106:12771–12775.
20. Rock JR, Randell SH, Hogan BL. Airway basal stem cells: a perspective on their roles in epithelial homeostasis and remodeling. *Dis Model Mech* 2010;3:545–556.
21. Bitron MD, Aharonson EF. Delayed mortality of mice following inhalation of acute doses of CH_2O, SO_2, Cl_2, and Br_2. *Am Ind Hyg Assoc J* 1978;39:129–138.
22. Basset F, Ferrans VJ, Soler P, Takemura T, Fukuda Y, Crystal RG. Intraluminal fibrosis in interstitial lung disorders. *Am J Pathol* 1986;122:443–461.
23. Rock JR, Hogan BL. Epithelial progenitor cells in lung development, maintenance, repair, and disease. *Annu Rev Cell Dev Biol* 2011;27:493–512.
24. Musah S, Chen J, Hoyle GW. Repair of tracheal epithelium by basal cells after chlorine-induced injury. *Respir Res* 2012;13:107.
25. Puchelle E, Zahm JM, Tournier JM, Coraux C. Airway epithelial repair, regeneration, and remodeling after injury in chronic obstructive pulmonary disease. *Proc Am Thorac Soc* 2006;3:726–733.
26. Hajj R, Baranek T, Le Naour R, Lesimple P, Puchelle E, Coraux C. Basal cells of the human adult airway surface epithelium retain transit-amplifying cell properties. *Stem Cells* 2007;25:139–148.
27. Rock JR, Gao X, Xue Y, Randell SH, Kong YY, Hogan BL. Notch-dependent differentiation of adult airway basal stem cells. *Cell Stem Cell* 2011;8:639–648.
28. Daniels GM, Amara SG. Selective labeling of neurotransmitter transporters at the cell surface. *Methods Enzymol* 1998;296:307–318.

29. Liu X, Driskell RR, Engelhardt JF. Stem cells in the lung. *Methods Enzymol* 2006;419:285–321.
30. Hubbs AF, Goldsmith WT, Kashon ML, Frazer D, Mercer RR, Battelli LA, Kullman GJ, Schwegler-Berry D, Friend S, Castranova V. Respiratory toxicologic pathology of inhaled diacetyl in Sprague-Dawley rats. *Toxicol Pathol* 2008;36:330–344.
31. Ghanei M, Chilosi M, Mohammad Hosseini Akbari H, Motiei-Langroudi R, Harandi AA, Shamsaei H, Bahadori M, Tazelaar HD. Use of immunohistochemistry techniques in patients exposed to sulphur mustard gas. *Pathol Res Int* 2011;2011:659603.
32. Mo Y, Chen J, Schlueter CF, Hoyle GW. Differential susceptibility of inbred mouse strains to chlorine-induced airway fibrosis. *Am J Physiol Lung Cell Mol Physiol* 2013;304:L92–L102.
33. Costa CL, Spilborghs GM, Martins MA, Saldiva PH, Mauad T. Nitric acid–induced bronchiolitis in rats mimics childhood bronchiolitis obliterans. *Respiration* 2005;72:642–649.
34. Teisanu RM, Chen H, Matsumoto K, McQualter JL, Potts E, Foster WM, Bertoncello I, Stripp BR. Functional analysis of two distinct bronchiolar progenitors during lung injury and repair. *Am J Respir Cell Mol Biol* 2011;44:794–803.